Human Exposure to the Near Field of Radiobase Antennas—A Full-Wave Solution Using Parallel FDTD

Luca Catarinucci, Paolo Palazzari, and Luciano Tarricone

***Abstract*—The problem of human exposure to the near field of radiobase antennas is a complex and challenging task. A numerical full-wave solution is highly recommended because of the accuracy needed. Unfortunately, the problem is computationally heavy. In this paper, a parallel finite-difference time-domain tool is proposed for the solution of the addressed problem so that the use of supecomputing platforms is combined with appropriate numerical human phantoms. Results demonstrate the good accuracy of the proposed solution. A detailed discussion is presented on the case of human exposure to real radiobase antennas, as well as on some critical issues concerning safety standards.**

***Index Terms*—Near field (NF), numerical phantom, parallel finite difference time domain (FDTD), radiobase antennas.**

I. Introduction

THE rapid diffusion of wireless technologies has focused attention on the potential risks for human health due to the exposure to electromagnetic (EM) fields. The problem, which is not new, is now a hot topic both for scientific research and for its political and social implications.

Among the several EM sources, a particular interest has been addressed, until now, to cellular phones [1], [2], while a much smaller emphasis has been reserved to radiobase-station antennas (RBAs) [3]–[5]. Nonetheless, the exposure to the near field (NF) of such devices is a relevant issue for a large class of workers, spending long daily time intervals in the proximity of RBAs (for instance, employees involved in radio-communication apparatus installation and maintenance or those working over building roofs hosting RBAs).

The NF interaction between RBAs and humans is a difficult problem. It has been attacked with experimental approaches [6], [7] using homogeneous or simplified human phantoms. For apparent reasons, such an approximation is far from providing results as accurate as required from the complexity of a liable health-risk evaluation. A numerical solution, on the other hand, is potentially attractive because of several accurate numerical phantoms developed in the recent past (as will be discussed below) and the large variety of rigorous numerical EM techniques proposed in the literature. Unfortunately, a numerical accurate solution is quite difficult because of the huge computational effort required. In fact, in many cases, panel RBAs have a leading dimension D of nearly 2 m, with consequent relevant far-field distances (using classical D^2/λ or $2D^2/\lambda$ relationships [8]). Therefore, the use of a full-wave solver, necessary for a rigorous NF analysis, is unaffordable with standard computational techniques. In this paper, a full-wave numerical solution is proposed for the exposure of human beings to the NF of real RBAs used for the GSM mobile system. The solution here proposed is based on the implementation of a finite-difference time-domain (FDTD) approach on a parallel computer of the APE/Quadrics family. The Yale human project (YHP) numerical phantom is used.

The paper is organized as follows. In Section II, the parallel FDTD approach is described, explaining the choice of the parallel computer platform, as well as the parallel algorithm. In Section III, a short review is given on the used numerical phantom. In Section IV, results are given, validating the proposed FDTD code, and estimating the human exposure to the NF of several real RBAs. Finally, conclusions are drawn.

II. Parallel FDTD on APE/Quadrics Platforms

The FDTD approach is quite well known and used for a large class of EM problems due to its high versatility. Yee's FDTD algorithm transforms the time-dependent Maxwell's curl equations into a set of finite-difference relations that have the following properties [9], [10].

1) The space and time derivatives are approximated by using the central discretization, therefore, resulting in second-order accurate expressions.
2) The location of the electrical (E) and magnetic (H) fields in the Yee grid implicitly enforce the Maxwell's divergence equations.
3) The time-stepping process is fully explicit and the algorithm is nondissipative (numerical wave modes propagating in the mesh do not decay because of nonphysical effects due to the time-stepping algorithm).

A wide literature is available concerning the FDTD approach, and this is not the appropriate context for a detailed description of the method. We can just recall here that, among the several possible boundary conditions [11]–[13], Mur's absorbing boundary conditions (ABCs) are used. In fact, even though a

Manuscript received March 6, 2002; revised October 3, 2002. This work was supported in part by the CNR-Agenzia 2000.

L. Catarinucci is with the Dipartimento di Ingegneria Elettronica e dell' Informazione, Universita di Perugia, Perugia 06125, Italy and also with the Dipartimento di Ingegneria dell' Innovazione, Universita di Lecce, Lecce 73100, Italy (e-mail: luca.catarinucci@unile.it).

P. Palazzari is with the Computing and Modeling Department, Italian National Agency for New Technologies, Energy, and Environment (ENEA), Rome 00100, Italy (e-mail: palazzari@casaccia.enea.it).

L. Tarricone is with the Dipartimento di Ingegneria dell' Innovazione, Universita di Lecce, Lecce 73100, Italy (e-mail: luciano.tarricone@unile.it).

Digital Object Identifier 10.1109/TMTT.2003.808695

perfectly matched layer (PML) ABC can be more accurate, they are more time consuming, and their implementation on parallel architectures such as the ones adopted here is not at all trivial. Anyway, Mur's ABCs guarantee an accuracy appropriate for the problem, as demonstrated below.

Moreover, the classical relationships reported in [9] and [10] are used to guarantee spatial and time stability.

A. Choice of the Parallel Architecture and Parallel Implementation

The elected architecture is the APE/Quadrics series [14]–[17]. It is a so-called single-instruction multiple-data (SIMD) platform. A SIMD platform is a multiprocessor architecture where every processor performs the same operation on different data in the mean time.

The SIMD philosophy of APE/Quadrics machines is quite amenable for an efficient parallel implementation of the FDTD scheme, which has the following relevant characteristics:

1) it is synchronous;
2) all the processors execute the same instructions on different domains;
3) it needs interprocessor communications executed in a synchronous way;
4) it has regular patterns for memory accesses so deep memory hierarchies are not required.

The scheme of the parallel algorithm is given in the following:

FDTD Parallel Algorithm

begin FDTD algorithm

Choose a spatial discretization of the domain (Δx, $\Delta y, \Delta z$); if the domain has dimensions ($L_x \times L_y \times L_z$), the grid has $N_i \times N_j \times N_k$ points, being $N_{i,j,k} = (L_{x,y,z})/(\Delta_{x,y,z})$.

Determine the time step Δt;

Partition the whole rectangular domain $D = [N_i \times N_j \times N_k]$ into $P = P_i \times P_j \times P_k$ rectangular subdomains $D' = [N_i' \times N_j' \times N_k']$, being P_i, P_j, and P_k the number of processors along dimension i, j and k, and $N_i' = (N_i/P_i)$, $N_j' = (N_j/P_j)$ and $N_k' = (N_k/P_k)$ the dimension (expressed as number of grid points) of the generic subdomain D'.

for $(t = 0; t < T_{\rm end}; t = t + \Delta t)$

in all the processors do

compute the new values of H

communicate the H values on the boundary of each subdomain to its neighbor

compute the new values of E

enddo in all

put the correct value in the feed point in the processors containing the source;

in the boundary processors do compute the absorbing boundary conditions;

in all the processors communicate the E values on the boundary of each subdomain to its neighbor;

endfor

end FDTD algorithm.

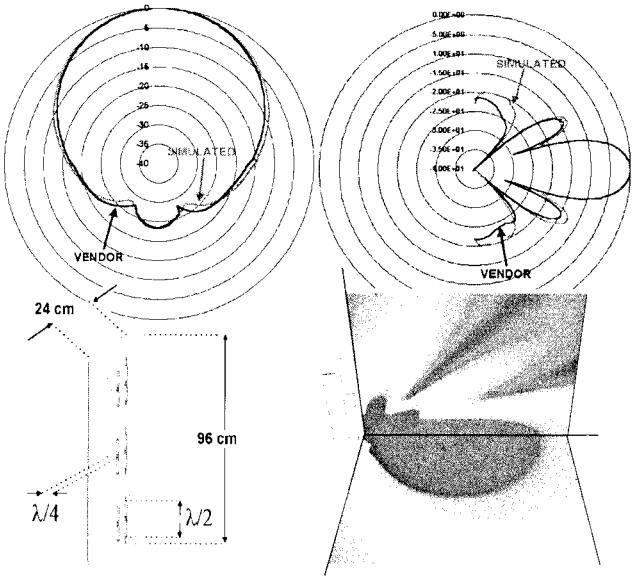

Fig. 1. H and E-plane RPs for RBA K730685. The graph reports E-field levels. Data for the simulated antenna are available via the Web. [Online]. Available: http://www.kathrein.de/en/mca/.

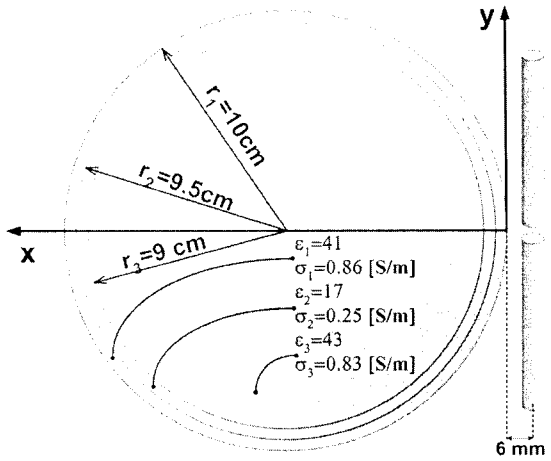

Fig. 2. Simulation scheme and adopted reference system for the three-layer sphere exposure to a 900-MHz half-wave dipole.

The implementation of the proposed algorithm on the APE/Quadrics architecture guarantees very high speed-ups, as well as the possibility of managing large memory requirements.

III. Numerical Phantoms

The story of the development of accurate numerical phantoms is rich and long, and we direct the interested reader to the specialized literature [18]–[21]. In this paper, we refer to one of the most appreciated phantoms, the one proposed at Yale University, New Haven, CT. Yale phantom derives from the segmentation of the transmission computerized (CT) X-ray thermography torso + head and magnetic resonance imaging (MRI) head slices of two living human males. The manually segmented 129 X-ray CT transverse slices were used to create a computerized three-dimensional volume array modeling all major internal structures of the body. The original X-ray CT images were reconstructed in a 512×512 matrix with a resolution of 1 mm in the x, y-plane. The z-axis resolution is

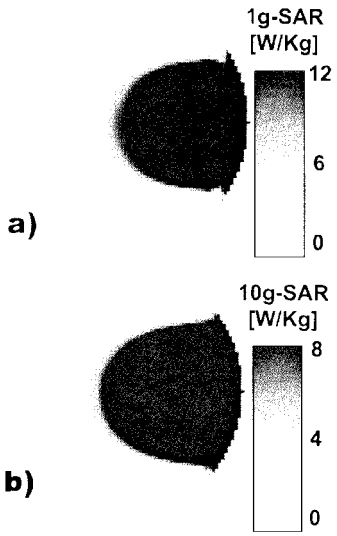

Fig. 3. (a) 1-g SAR levels and (b) 10-g SAR levels in the vertical plane of the exposed three-layer sphere.

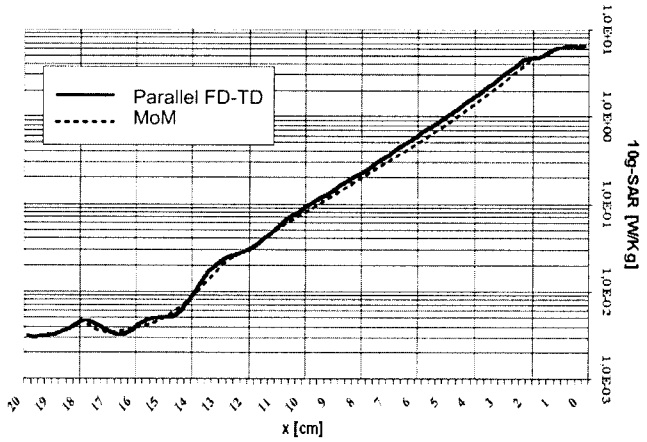

Fig. 4. 10-g SAR behavior along the x-axis using two different computational methods, which is proposed here parallel to the FDTD method and method of moments (MoM) [22]. The input power is 1 W.

1 cm from neck to mid-thigh and 0.5 cm from neck to crown of the head. The final torso + head phantom is created with a $128 \times 128 \times 243$ byte volume, giving a $4 \times 4 \times 4$ cubic mm voxel size dimension. Each voxel of the volume contains an index number designating it as belonging to a given organ or internal structure. The organ numbers and conductivity values at a working frequency of 900 MHz can be found in the cited literature.

IV. Results

A. FDTD Validation

In order to validate the proposed parallel FDTD code, in Fig. 1, we present the estimated radiation pattern (RP) evaluated for the RBA Kathrein (K) 730685, dimensions for which are also reported in Fig. 1. Results are attained by evaluating the radiated power density at a distance of 6 m for a working frequency of 902.5 MHz. No NF/far-field transformations are needed, the solution being completely full wave. A grey-level representation of the levels of the electric field in both the vertical and horizontal planes is also reported. It can be observed that the accuracy is satisfactory both in the H- and E-plane.

As further validation, several simulations have been performed in order to evaluate the dosimetric parameters for the most typical canonical cases. For instance, the exposure to the EM field of a 900-MHz half-wave dipole has been studied

TABLE I
Homogeneous Sphere Exposure to 1-W Half-Wave Dipole

Homogeneous sphere	
Antenna Input Power	1W
Power absorbed by the Homog. sphere	0.70W
Max SAR averaged over 1g	13.30W/Kg
Max SAR averaged over 10g	8.41 W/Kg

TABLE II
Three-Layer Sphere Exposure to 1-W Half-Wave Dipole

3-layered sphere	
Antenna Input Power	1W
Power absorbed by the 3-layered sphere	0.73W
Max SAR averaged over 1g	12.07W/Kg
Max SAR averaged over 10g	7.89 W/Kg

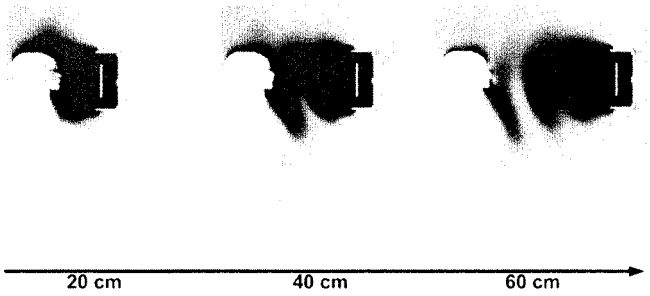

Fig. 5. E-field levels in a vertical plane simulation domain for three observation distances (white for low level fields, black for high level fields). The antenna (K730678) and the human shape are clearly identifiable. Emitted power is 32 W.

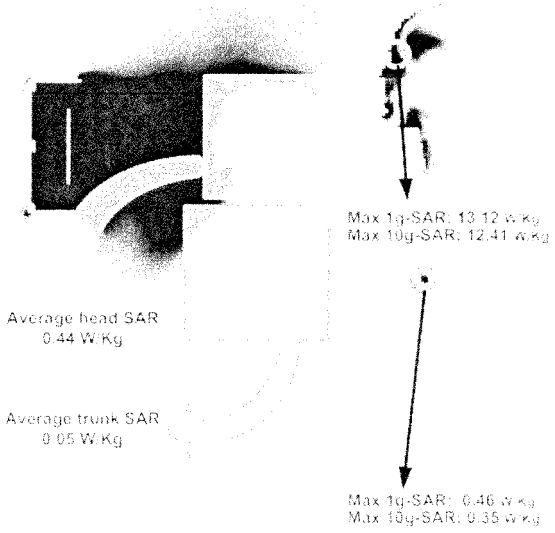

Fig. 6. NF exposure to K730678 RBA. Black regions correspond to high-intensity E-fields. Maximum SAR values in the head and trunk regions are reported on the right-hand side. The human–antenna distance is 30 cm.

TABLE III
PEAK SAR VALUES VARYING THE OBSERVATION DISTANCE. THE ANTENNA RADIATED POWER IS 32 W

1g-SAR and 10g-SAR: peak values				
	Heterogeneous phantom		Homogeneous Phantom	
distances	1g-SAR [W/Kg]	10g-SAR [W/Kg]	1g-SAR [W/Kg]	10g-SAR [W/Kg]
20 cm	29.30	14.79	30.02	19.11
30 cm	13.12	6.56	12.42	7.10
40 cm	10.50	5.23	9.85	5.61
50 cm	5.24	2.60	4.84	2.76
60 cm	4.67	2.30	4.34	2.47

for two simplified human head models (homogeneous sphere and three-layer sphere). For each analyzed case, the radiated power is 1 W, the external sphere radius is 10 cm, the feeding gap is 2.5 mm, and the distance between the feed and sphere surface is 6 mm. In Fig. 2, one of the implemented simulation schemes and the relative reference system are schematized. The local specific absorption rate (SAR), the SAR averaged over 1 g of tissue (1-g SAR), and over 10 g of tissue (10-g SAR) have been evaluated, and the power absorbed by the head has been estimated. For example, we now present the result for the exposure of the three-layer sphere (skin + bone + brain) to the half-wave dipole. In Fig. 3, both the 1- and 10-g SAR levels are represented in the main horizontal sphere section, while in Fig. 4, the behavior of the 10-g SAR along the x-axis (see Fig. 2) is represented and compared with data reported in [22].

Finally, the power absorbed by the sphere and the peak SAR values are reported in Tables I and II for both the homogeneous sphere and the three-layer one, respectively. The results show that almost 73% of the radiated power is absorbed by the spheres, which is in good agreement with data reported in [2].

B. Human Exposure to the NF of RBA

In Fig. 5, we report the qualitative E-field levels for the exposure of the heterogeneous YHP phantom, described in Section III, to a real radiobase antenna (K730678). The leading antenna dimension is $D = 30$ cm, while the emitted power is 32 W. Three different exposure distances are represented. The implemented simulation schemes need large simulation domains that require almost 2 GB of RAM for the memorization and almost 104 GFlop for the fields evaluation. Nevertheless, using an optimized code for the Quadrics/APE100 machine, less than 1 h is necessary to complete the simulation. As shown in Figs. 5 and 6, the E and H values can be locally evaluated with a spatial resolution in the millimeter scale, as well as all the relevant dosimetric parameters, such as the SAR. In Fig. 6, we report the maximum SAR value, as well as the average SAR values attained over two different zones (the head and trunk regions). Such values can be compared with the safety limits assumed by the International Commission on Non-Ionizing Radiation Protection (ICNIRP) standard for workers:

1) whole body average SAR: 0.4 W/kg;
2) 10-g SAR in each head or trunk point: 10 W/kg;
3) 10-g SAR in each limb point: 20 W/kg.

As is apparent from this figure, such limits are not exceeded when referring to the averaged values. Nonetheless, local SAR values are not negligible, as easily noticed in Fig. 6, and enforce a more detailed discussion about the consideration of local SAR estimation.

Furthermore, the ability to give a dosimetric estimation over large human tissue portions, as well as in small regions, can be successfully exploited to verify the accuracy of several experimental setups using a homogeneous phantom approximation. In order to do this, the human exposure problem has been solved using two different numerical phantoms: the YHP heterogeneous phantom and a homogeneous phantom with the same shape as the YHP one, though modeled with constant dielectric characteristics in each point ($\varepsilon_r = 43$ and $\sigma = 0.83$ S/m).

The phantoms have been exposed to the K730678 antenna, varying mutual position and distance. For each simulation, the following parameters have been estimated:

1) local SAR, 1-g SAR, and 10-g SAR, in each point of the studied phantoms;
2) peak SAR for both 1- and 10-g SAR, in the phantoms' head and trunk;
3) power absorbed by the phantoms.

In Table III, the peak values of the 1- and 10-g SAR are reported for five different distances between human and source. A comparison between the results related to the heterogeneous case (first and second column) and the homogeneous ones (third and fourth column), reports similar values, except in the case of small phantom–source distance. Similar observations can be made for the results summarized in Table IV, where the SAR values averaged over a thin vertical head portion are reported. The presented results and some others omitted for brevity, therefore, show that the dosimetric parameters evaluated for a homogeneous phantom are comparable with the heterogeneous data. Nevertheless, as is easily predictable, a detailed comparison shows substantial differences between the use of the homogeneous phantom rather than the heterogeneous one.

For instance, for a human–antenna distance of 30 cm, the estimated peak 1-g SAR is 13.12 W/kg for the YHP phantom versus 12.42 W/kg for the homogeneous one (see Fig. 7). The SAR averaged over a large portion of the head is also comparable (0.39 W/kg versus 0.35 W/kg), but a maximum absolute difference of almost 4 W/kg has been calculated for the 1-g SAR estimation, and this is because of the different position of the local maxima and minima, as shown in Fig. 7. In Fig. 8 and Table V, we report the absolute difference of the SAR local evaluation between the two studied phantoms in order to give an estimation of the possible error caused by the homogenous approximation. It can be observed that, when increasing the observation distance, the absolute difference is reduced, even though the overall percentage error is rather constant.

TABLE IV
SAR AVERAGED OVER A THIN HEAD PORTION. THE ANTENNA RADIATED POWER IS 32 W

SAR averaged over a thin vertical head portion				
	Heterogeneous phantom		Homogeneous Phantom	
distances	1g-SAR [W/Kg]	10g-SAR [W/Kg]	1g-SAR [W/Kg]	10g-SAR [W/Kg]
20 cm	1.515	1.457	2.245	2.381
30 cm	0.393	0.380	0.354	0.372
40 cm	0.328	0.317	0.293	0.307
50 cm	0.176	0.171	0.155	0.284
60 cm	0.165	0.160	0.145	0.140

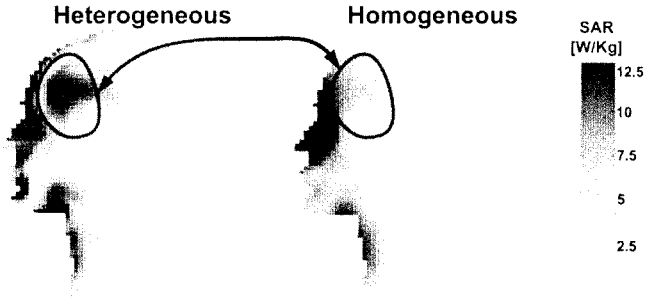

Fig. 7. 1-g SAR levels in the phantoms' head for the simulation scheme represented in Fig. 6. A zone with high SAR differences is marked.

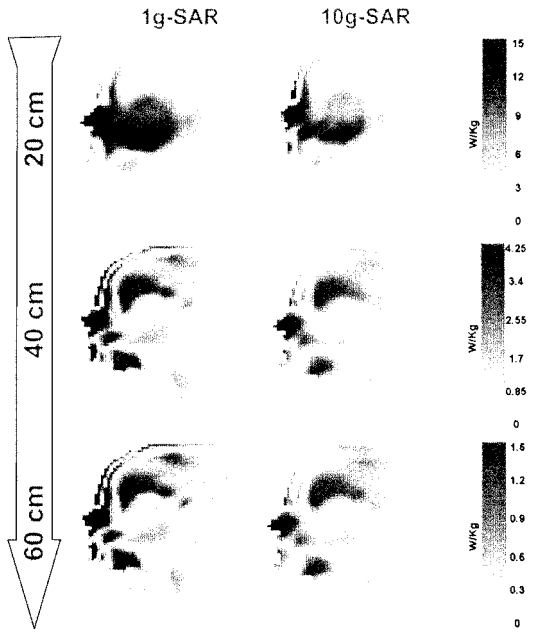

Fig. 8. Absolute SAR difference between YHP and homogeneous phantom. Both the 1-g SAR difference (left-hand-side column) and the 10-g SAR difference (right-hand-side column) have been reported.

Nevertheless, the error distribution is not uniform, and this makes the definition of a correction factor valid in every point of the target complicated.

The obtained results can be summarized as follows:

- both the position and value of the maximum evaluated SAR are similar in the studied phantoms for each RBA-phantom distance and mutual position;

TABLE V
ABSOLUTE MAXIMUM SAR VALUES DIFFERENCES BETWEEN HOMOGENEOUS AND HETEROGENEOUS RESULTS. THE ANTENNA RADIATED POWER IS 32 W

Maximum homogeneous Vs heterogeneous SAR absolute difference		
distances	1g-SAR difference [W/Kg]	10g-SAR difference [W/Kg]
20 cm	13.55	7.91
30 cm	4.07	2.15
40 cm	3.19	1.69
50 cm	1.58	0.83
60 cm	1.42	0.75

- values of the SAR averaged over a large portion of human body, like the head or a portion of it, the bust or the trunk, are comparable in both cases;
- comparison of the local values of the dosimetric parameters instead puts forward substantial differences between the use of a heterogeneous phantom rather than a homogeneous one. A 40% difference, in some investigated phantom's points, can be observed.

V. CONCLUSION

In this paper, a full-wave solution, based on a parallel FDTD method, has been proposed for the problem of human exposure to the NF of radiobase antennas. The problem, relevant for several classes of workers, is also a challenging effort from an EM and numerical point-of-view.

Results proposed in this paper suggest that the approach of parallel FDTD, combined with the use of accurate numerical human phantoms, is appropriate. The current safety standards are typically not exceeded even for very small human–antenna distances, even though the attained results suggest a careful analysis of local peak values, as well as a conscious use of experimental approximations such as homogeneous phantoms.

REFERENCES

[1] A. D. Tinniswood, C. M. Furse, and O. P. Gandhi, "Computations of SAR distributions for two anatomically based models of the human head using CAD files of commercial telephones and the parallelized FDTD code.," *IEEE Trans. Antennas Propagat.*, vol. 46, pp. 829–833, June 1998.

[2] K. Nikita *et al.*, "A study of uncertainties in modeling antenna performance and power absorption in the head of a cellular phone user," *IEEE Trans. Microwave Theory Tech.*, vol. 48, pp. 2676–2686, Dec. 2000.

[3] G. Lazzi and O. P. Gandhi, "A mixed FDTD-integral equation approach for on-site safety assessment in complex electromagnetic environments," *IEEE Trans. Antennas Propagat.*, vol. 48, pp. 1830–1836, Dec. 2000.

[4] P. J. Dimbylow, "FDTD calculations of the whole body averaged SAR in an anatomically realistic voxel model of the human body from 1 MHz to 1 GHz," *Phys. Med. Biol.*, vol. 42, pp. 479–490, 1997.
[5] P. Bernardi, M. Cavagnaro, S. Pisa, and E. Piuzzi, "Human exposure to radiobase station antennas in urban environment," *IEEE Trans. Microwave Theory Tech.*, vol. 48, pp. 1996–2003, Nov. 2000.
[6] A. Bahr, D. Manteuffel, and D. Heberling, "Occupational safety in the near field of a GSM base station," in *Proc. IEEE AP-S*, Davos, Switzerland, Apr. 2000, Paper 3A6.7.
[7] K. Ito, L. Hamada, T. Asahina, and H. Yoshimura, "Phantoms for estimation of interaction between antenna and human body," in *Proc. IEEE AP-S*, Davos, Switzerland, Apr. 2000, Paper 3A6.8.
[8] J. D. Kraus, *Antennas*. New York: McGraw-Hill, 1988.
[9] A. Taflove and M. E. Brodwin, "Numerical solution of steady-state electromagnetic scattering problems using the time-dependent Maxwell's equations," *IEEE Trans. Microwave Theory Tech.*, vol. MTT-23, pp. 623–630, Aug. 1975.
[10] A. Taflove, *Computational Electrodynamics: The Finite-Difference Time-Domain Method*. Norwood, MA: Artech House, 1995.
[11] G. Mur, "Absorbing boundary conditions for the finite-difference approximation of the time-domain electromagnetic-field equations," *IEEE Trans. Electromagn. Compat.*, vol. EMC-23, pp. 377–382, Nov. 1981.
[12] J.-P. Berenger, "A perfectly matched layer for the absorption of electromagnetic waves," *J. Comput. Phys.*, vol. 114, 1994.
[13] ——, "A perfectly matched layer for the FDTD solution of wave-structure interaction problems," presented at the IEEE AP-S Symp., 1996.
[14] A. Bartoloni *et al.*, "A hardware implementation of the APE100 architecture," *Int. J. Modern Phys.*, vol. C4, 1993.
[15] P. Palazzari, "Heterogeneity as key feature for high performance computing: The PQE1 prototype," in *Proc. IEEE Heterogeneous Computing Workshop*, Cancun, Mexico, May 1, 2000.
[16] APE: The Italian SIMD Supercomputer in the Teraflop Range [Online]. Available: http://chimera.roma1.infn.it/ape.html
[17] C. Battista, "The APE100 computer: (I) the architecture," *Int. J. High Speed Comput.*, no. 5, 1993.
[18] I. G. Zubal, C. R. Harrell, E. O. Smith, Z. Rattner, G. Gindi, and P. B. Hoffer, "Computerized 3-dimensional segmented human anatomy," *Med. Phys.*, vol. 21, no. 2, pp. 299–302, Feb. 1994.
[19] C. Gabriel, S. Gabriel, and E. Corthout, "The dielectric properties of biological tissues: I literature survey," *Phys. Med. Biol.*, vol. 41, pp. 2231–2249, 1996.
[20] C. Gabriel, "Compilation of the dielectric properties of body tissues at RF and microwave frequencies," Brooks Air Force Base, Tech. Rep. AL/OE-TR-1996-0037, 1996.
[21] P. A. Mason, "Effects of frequency, permittivity and voxel size on predicted SAR values in biological tissues during EMF exposure," *IEEE Trans. Microwave Theory Tech.*, vol. 48, pp. 2050–2061, Nov. 2000.
[22] K. Nikita, G. Stamatakos, N. Uzunoglu, and A. Karafotias, "Analysis of the interaction between a layered spherical human head model and a finite-length dipole," *IEEE Trans. Microwave Theory Tech.*, vol. 48, pp. 2003–2013, Nov. 2000.

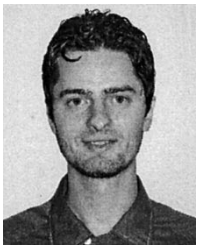

Luca Catarinucci was born in Todi, Perugia, Italy, on November 28, 1972. He received the Laurea degree (with honors) from the Universita di Perugia, Perugia, Italy, in 1998. His Laurea thesis concerned the optimization of the frequency assignment on radiobase antennas for the cellular global system for mobile communications (GSM) network.

He is currently a Contract Researcher with the Interuniversity Centre on the interaction between ElectroMagnetic fields and Biosystems (ICEMB), Genova, Italy. He is also with the Dipartimento di Ingegneria Elettronica e delle' Informazione (DIEI), Universita di Perugia, and with the Dipartimento di Ingegneria dell' Innovazione (DII), Universita di Lecce, Italy. He is currently involved in the FDTD analysis of human–antenna interaction and EM parallel computing.

Paolo Palazzari received the Laurea degree in electronic engineering and Ph.D. degree from "La Sapienza" University of Rome, Rome, Italy, in 1989 and 1994, respectively.

He was Scientific Collaborator of the Electronic Engineering Department, University "La Sapienza," Rome, Italy, until 1996, when he joined the Italian National Agency for New Technologies, Energy, and Environment (ENEA), Rome, Italy, as Researcher with the Computing and Modeling Department. His main research topics are related to design and programming of parallel architectures, high-level synthesis techniques, and nonlinear optimization techniques.

Luciano Tarricone was born in Galatone, Lecce, Italy, on May 24, 1966. He received the Laurea degree (with honors) in electronic engineering and the Ph.D. degree from Rome University "La Sapienza," Rome, Italy, in 1989 and 1994, respectively. Both his Laurea and Ph.D. theses were focused on the biological effects of EM fields and electromagnetic compatibility (EMC).

In 1990, he was a Visiting Researcher with the Italian National Institute of Health Laboratories, where he was in charge of European draft standards for electromagnetic interferences (EMIs) with implanted devices. From 1990 to 1992, he was a Researcher with the IBM Rome Scientific Centers. From 1992 to 1994, he was with the IBM European Center for Scientific and Engineering Computing, Rome, Italy, where he was involved in supercomputing for several scientific applications. Since 1994, he has been a Researcher with Department of Information Engineering, Universita di Perugia, Perugia, Italy, and since 1998, he has been a Professore Incaricato of EM fields and EMC. Since November 2001, he has also been a faculty member with the Department of Innovation Engineering, University of Lecce, Lecce, Italy. He has authored approximately 150 scientific papers. His main contributions are in the modeling of microscopic interactions of EM fields and biosystems, and in numerical methods for efficient computer-aided design (CAD) of microwave circuits and antennas. He is currently involved in the FDTD analysis of human–antenna interaction, graph-theory methods for the enhancement of numerical EM techniques, novel CAD tools and procedures for MW circuits, and EM parallel computing.